Editors' Suggestion

Enhanced Interactions between Dipolar Polaritons

Emre Togan,[1] Hyang-Tag Lim,[1] Stefan Faelt,[1,2] Werner Wegscheider,[2] and Atac Imamoglu[1]
[1]Institute of Quantum Electronics, ETH Zurich, CH-8093 Zurich, Switzerland
[2]Solid State Physics Laboratory, ETH Zurich, CH-8093 Zurich, Switzerland

(Received 13 July 2018; revised manuscript received 16 October 2018; published 26 November 2018)

Nonperturbative coupling between cavity photons and excitons leads to the formation of hybrid light-matter excitations, termed polaritons. In structures where photon absorption leads to the creation of excitons with aligned permanent dipoles, the elementary excitations, termed dipolar polaritons, are expected to exhibit enhanced interactions. Here, we report a substantial increase in interaction strength between dipolar polaritons as the size of the dipole is increased by tuning the applied gate voltage. To this end, we use coupled quantum well structures embedded inside a microcavity where coherent electron tunneling between the wells creates the excitonic dipole. Modifications of the interaction strength are characterized by measuring the changes in the reflected light intensity when polaritons are driven with a resonant laser. The factor of 6.5 increase in the interaction-strength-to-linewidth ratio that we obtain indicates that dipolar polaritons could constitute an important step towards a demonstration of the polariton blockade effect, and thereby to form the building blocks of many-body states of light.

DOI: 10.1103/PhysRevLett.121.227402

The realization of strongly interacting photonic systems is one of the holy grails of quantum optics. Substantial progress towards this goal has been achieved using Rydberg polaritons—quasiparticles consisting of a propagating photon and a collective Rydberg excitation: van der Waals interactions between Rydberg atoms ensure that the polaritonic excitations interact strongly [1–6]. In solid-state cavity-polariton systems consisting of a cavity photon and a quantum well exciton, dominant direct exciton (DX) interactions originate from short-range exchange terms [7,8]. These interactions have led to the manifestation of a number of intriguing collective phenomena, ranging from the formation of spontaneous coherence [9] through the observation of vortex-antivortex pairs [10,11] and dark solitons [12,13] to the realization of the polariton Josephson effect [14,15]. However, a mean-field approach could be used to accurately describe all these observations. Very recently, photon correlation measurements on strongly confined polaritons have demonstrated weak quantum correlations [16,17].

Increasing polariton-polariton interaction further is crucial to exploring a new regime of strongly correlated photons. One way to enhance interactions is to engineer polaritonic excitations with a permanent dipole moment [18]: such dipolar polaritons emerge as elementary optical excitations when DXs in a quantum well (QW) are strongly coupled to both microcavity photons and indirect excitons (IXs) with a permanent dipole moment. Prior theoretical studies have predicted different factors for enhancement of the interactions between polaritons as the IX content is varied [19,20]. A recent experimental measurement of interactions between polaritons with induced dipoles in a wide QW has reported a much larger enhancement [21] compared to the prediction of the theoretical studies. In this Letter, we use pulsed resonant excitation of polaritons and the resulting blue shift to determine the polariton interaction strength as a function of IX content. By choosing a low-duty cycle, we ensure that slow laser-induced changes in the charge environment have a small contribution to the extracted interaction strength. The structure we employ in our experiment allows us to tune the IX content and to increase the ratio of the interaction strength of polaritons to their linewidth without substantially compromising the exciton-photon coupling strength. As we demonstrate in this Letter, the associated dipole-dipole interactions can be much stronger than the intrinsic interactions between DXs and thereby provide a promising platform to realize many-body states of photons [22].

We work with a microcavity sample, illustrated in Fig. 1(a), which contains three pairs of coupled $In_{0.04}Ga_{0.96}As$ QWs embedded inside a p-i-n diode. By applying a voltage (V_G) between the p and n doped regions, we control the electric field E_z in the growth direction and adjust the detuning between different QW exciton states. A DX state localized on the thick (11 nm) QW experiences a quantum-confined Stark shift, and its energy decreases quadratically with the applied electric field. The same electric field leads to a linear shift in energy of an IX state with the hole localized on the thick QW and the electron on the thin (5 nm) QW. Separated by a thin (13 nm) GaAs layer, the proximity of the two QWs facilitates electron tunneling with a rate $J = 3.5$ meV between the two wells. When the energy of the DX state and the IX state are equal, this tunneling hybridizes the

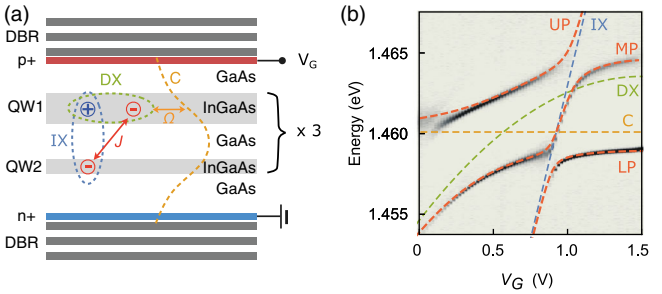

FIG. 1. (a) Schematic of the sample structure. The sample contains three pairs of $In_{0.04}Ga_{0.96}As$ coupled quantum wells (QWs) located at three separate antinodes of a $5\lambda/2$ cavity formed between two GaAs/AlAs distributed Bragg reflectors (DBRs). To ensure that electron tunneling for the lowest-energy electron states of the two QWs occur at finite electric field, we use QWs with different thicknesses; thus each pair consists of a 5-nm- and a 11-nm-thick QW. The thickness of the GaAs barrier between the two QWs is 13 nm. An electric potential V_G applied between the p (66 nm) and n (66 nm) doped layers tunes the energy of the direct exciton (DX) and indirect exciton (IX) levels. See the Supplemental Material [23] for details on the sample structure and the fabrication process. (b) Reflection spectrum with zero in-plane momentum excitation ($\mathbf{k}_{\mathrm{in}} = 0$) as a function of applied gate voltage V_G. Changes in the energy levels of the bare DX (green dashed line) and IX (blue dashed lines) are extracted from a measurement of the reflection spectrum at a point where the top DBR has been etched (see the Supplemental Material [23]). Cavity resonance (orange dashed line) is constant as we vary V_G. Changes in the energies of the three coupled states—upper polariton (UP), middle polariton (MP), and lower polartion (LP)—with V_G are shown as red dashed lines. We use the calculated eigenstates associated with the red lines to estimate the DX, IX, and C (cavity) content at a particular sample position and V_G.

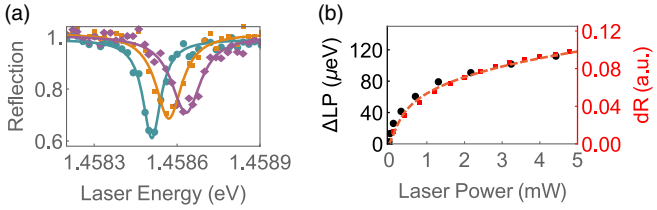

FIG. 2. (a) Reflection spectrum obtained at $V_G = 1.1$ V when scanning a weak (~0.5 μW) linearly polarized probe laser across a LP resonance. The power of a second, orthogonally linearly polarized pump laser tuned to 1.45853 eV is varied (cyan: 0 mW, orange: 2.15 mW, purple: 7.2 mW). The polariton linewidth broadens as we increase the pump power: the γ_P values are 80 μeV, 116 μeV, and 130 μeV, respectively. (b) The left axis shows changes in the LP resonance energy, extracted from traces as shown in (a), as the power of the pump laser (horizontal axis) is varied. The right axis shows changes in the differential reflection of the pump laser tuned to 1.45853 eV as its power is varied. Differential reflection (dR) is obtained by subtracting the reflection signal obtained at $V_G = 1.1$ V from a reflection trace obtained at $V_G = 0$ V. The red dashed line shows the calculated dR signal using Eq. (2). The pump laser is off resonant with all polariton transitions at $V_G = 0$ V. All reflection and pump-probe experiments are carried out using a pulse scheme to minimize the effects of light-induced slow changes to the polariton environment (see the Supplemental Material [23]).

two exciton states. Due to its large oscillator strength, the DX state also couples strongly to the cavity mode localized between the two distributed Bragg reflectors (DBRs) at a rate Ω. The Hamiltonian of the coupled system for a zero in-plane wave vector $\mathbf{k}_{\mathrm{in}} = 0$ can be written in the matrix form

$$H = \begin{pmatrix} \epsilon_{\mathrm{IX}} - edE & J/2 & 0 \\ J/2 & \epsilon_{\mathrm{DX}} - \alpha E^2 & \Omega/2 \\ 0 & \Omega/2 & \epsilon_{\mathrm{C}} \end{pmatrix}, \qquad (1)$$

where e is the elementary charge, d is the IX dipole size, α is the polarizability of DX, ϵ_{DX} and ϵ_{IX} are the zero-electric-field energies of the DX and IX states, and ϵ_{C} is the energy of the cavity mode at $\mathbf{k}_{\mathrm{in}} = 0$. We assume that the coupling between the IX state and cavity mode is negligible. The quasiparticle compositions of the eigenstates, named the lower, middle, and upper polariton modes, are characterized by generalized Hopfield coefficients x, y, and c so that an eigenstate can be written as $x|\mathrm{DX}\rangle + y|\mathrm{IX}\rangle + c|\mathrm{C}\rangle$, where $|x|^2 + |y|^2 + |c|^2 = 1$.

We probe the sample held at 4 K by focusing our illumination beam down to a ~5 μm spot and observing changes in the reflection of the illumination beam. As shown in Fig. 1(b), the reflection spectrum is dominated by three modes that we identify as the three polariton modes. The energies of the three polariton modes agree well with the eigenvalues of the matrix in Eq. (1) with $d = 21$ nm, $\alpha = 1.2 \times 10^{-15}$ eV m^2 V^{-2}, $\epsilon_{\mathrm{IX}} = 1.48209$ eV, $\epsilon_{\mathrm{DX}} = 1.46354$ eV, $\epsilon_{\mathrm{C}} = 1.4601$ eV, and $\Omega = 4.6$ meV. We use coefficients x, y, and c that we extract from this model to identify DX, IX, and C (cavity) content for different polariton modes as a function of V_G. We will focus on the lower polariton for the rest of this Letter.

Figure 2(a) illustrates the reflection spectrum obtained when the frequency of a low-power (~0.5 μW) linearly polarized laser, that we call the probe laser, is scanned across a lower polariton resonance with $|x|^2 = 0.27$, $|y|^2 = 0.01$, and $|c|^2 = 0.72$ ($V_G = 1.1$ V). The polariton resonance blueshifts as the intensity of a second, orthogonally polarized laser tuned to the unperturbed polariton resonance (1.45853 eV) is increased. We refer to this second laser as the pump laser. The blueshift, which is initially linear with the intensity of the pump laser, saturates for high intensities [Fig. 2(b)]. We measure the shift of the polariton resonance by setting a polarizer such that only the probe laser is detected on the detector. The frequency of the pump laser is fixed, and is not tuned as a function of

pump-laser intensity. The magnitude of the differential reflection of the pump laser also exhibits saturation with power [Fig. 2(b)]. This saturation behavior, in the optical limiter regime, is measured when the polarizer is tuned to detect the reflected pump laser. We use this saturation behavior of the pump laser to characterize the nonlinearity of the polariton mode.

To quantitatively extract the strength of the nonlinearity, we model the polariton system, in the mean field limit, by a single nonlinear mode with a Kerr-like nonlinearity [28]. Within this approximation, the equation of motion for the lower polariton annihilation operator's expectation value ($p = \langle \hat{p} \rangle$) can be written as

$$\frac{dp}{dt} = -\left(\frac{\gamma_P}{2} + i\delta_P\right)p - ig_P|p|^2 p - c\sqrt{\gamma_{in}}\sqrt{I^{in}}, \quad (2)$$

where $\gamma_P = 103$ μeV is the position-averaged full width at half maximum (FWHM) polariton linewidth [see Fig. 3(b)], $\delta_P = \epsilon_{pol} - \epsilon_{laser}$ is the detuning of the laser from the polariton mode, $\gamma_{in} = \gamma_P/6$ characterizes the input coupling rate, and I^{in} is the photon flux that characterizes the input intensity of the pump laser. Note that we choose $\gamma_{in} = \gamma_P/6$ in order to match the depth (contrast) of the polariton resonance from reflection measurements as shown in Fig. 2(a). The nonlinear coefficient of the effective single mode is $g_P = U/A$, where U is the strength of the two-dimensional (2D) polariton interaction and $A \sim 7$ μm $\times$ 7 μm denotes the mode area. To determine the mode area A, we solve the Gross-Pitaevski equation (GPE) (see the Supplemental Material [23]). For the parameter range relevant for our experiments, the polariton spatial distribution is determined primarily by the excitation laser's size (5 μm FWHM), the finite polariton lifetime, and the effective mass of polaritons. With $\delta_P = 0$ and in steady state, an increase in the polariton population leads to a blueshift of the polariton resonance; hence as I^{in} increases, the blueshift leads to a saturation of the polariton population, as well as a saturation of the differential reflection signal. For each position and gate voltage we fit a value of g_P so that the calculated differential reflection signal matches the measured differential reflection signal (see the Supplemental Material [23]).

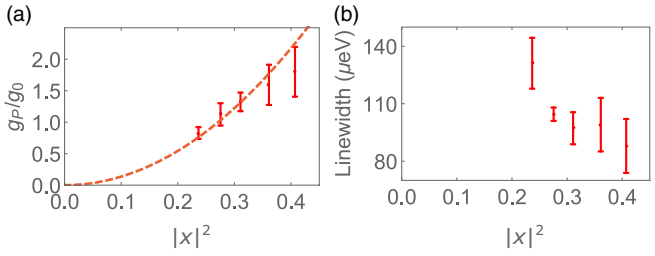

FIG. 3. (a) Changes in polariton interaction strength g_P extracted from differential reflection measurements similar to Fig. 2(b) as a function of $|x|^2$. Different data points were obtained at $V_G = 1.4$ V at different positions on the sample. The IX content remains $|y|^2 \leq 0.004$ for all of the data. Changes in g_P are in agreement with $g_P = (14 \pm 1)|x|^4 g_0$. The error bar for the parameter estimated in the model is based on the 1σ confidence interval obtained in the fit. The error bars on data points are standard deviations of the extracted g_P obtained at different repetitions of the experiment at different spatial positions that have the same $|x|^2$ content (See the Supplemental Material [23]). (b) Changes of the linewidth, in the linear regime, extracted from low-power (≤ 0.5 μW) reflection measurements using a single probe laser. The error bars are standard deviations of the extracted linewidth when repeating the experiment at different spatial positions that have the same $|x|^2$ content.

In order to demonstrate the utility and limitations of this method in characterizing the strength of the polariton nonlinearity, we measure changes of g_P for a fixed $V_G = 1.4$ V as we vary the cavity and DX contents. At this gate voltage, the IX content as well as the induced dipole moment of DX is negligible. We use the wedge that is present in the sample, which leads to position-dependent changes in ϵ_C, to vary the DX and cavity content of lower polaritons. Figure 3(a) illustrates the changes in the extracted g_P as a function of $|x|^2$ measured at different positions on the sample. The data are in agreement with $g_P = (14 \pm 1)|x|^4 g_0$, with $g_0 = 1.6$ neV. The $|x|^4$ dependence is the expected behavior for DX-induced polariton-polariton interactions [22]. We note that, for each data point, the standard deviations of the extracted g_P and polariton linewidth are large. These large variations in the extracted parameters are caused by residual effects of light-induced, position-dependent changes in the charge environment that lead to sublinewidth shifts of the polariton resonance. The experiments are carried out using a pulse sequence (10 ms long) with a low-duty-cycle laser exposure (250 ns long) to minimize the effect of slow changes in the polariton resonant frequency. Laser pulses lead to slow spectral shifts of the polariton resonance that persist for the sequence duration (10 ms) and lead to the laser being detuned from the polariton resonance by amounts that are position dependent. This additional, random contribution to detuning (δ_P) that is introduced in Eq. (2) alters the numerical estimate of g_P. Thus, an average over multiple positions with equal DX content but different δ_P's results in a large variation in the extracted g_P value. See the Supplemental Material [23] for more details on the pulse sequence and the characterization of these random spectral shifts, as well as estimates of the effects of these shifts on the estimated g_P.

At a fixed position, we then measure changes in g_P as we vary IX content by changing the V_G when the incident laser is either linearly or circularly polarized. As Fig. 4 illustrates, g_P increases by a factor of 5 as IX content increases from $|y|^2 = 0.002$ at $V_G = 1.4$ V to $|y|^2 = 0.14$ at $V_G = 0.95$ V. Remarkably, this substantial increase is independent of the polarization of the excitation laser. These results demonstrate that, by varying V_G, it is possible

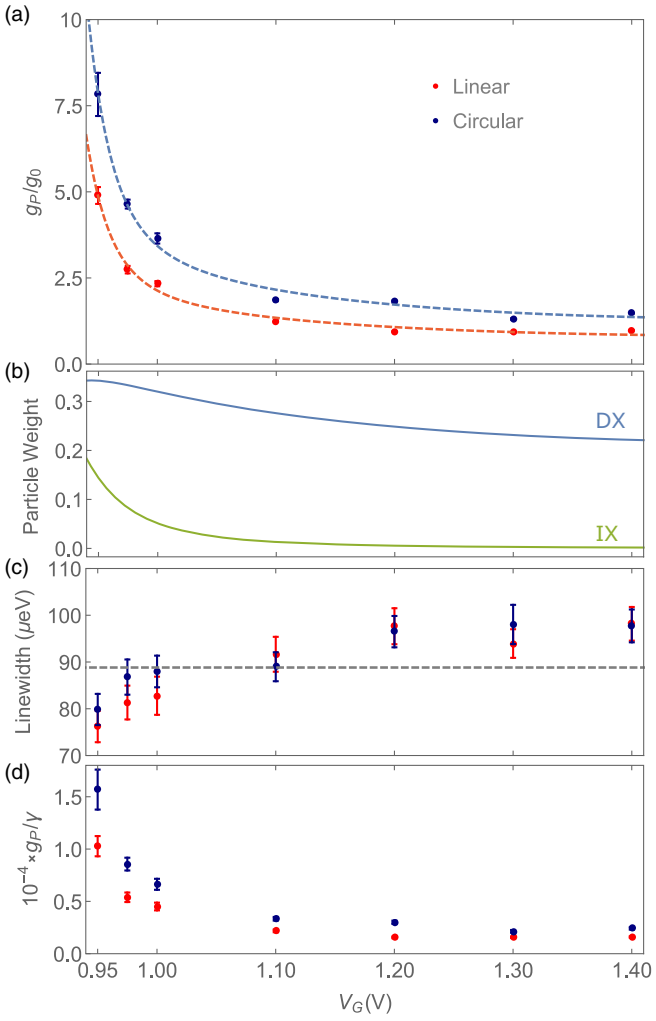

FIG. 4. (a) Changes in polariton interaction strength g_P extracted from differential reflection measurements similar to Fig. 2(b) as a function of V_G at a fixed position. The data match a simple model $g_P = a(|x|^4 + b|y|^4)g_0$ with $a = 17.6 \pm 0.1$, $b = 7.4 \pm 0.5$ for linearly polarized measurements (red dashed line) and $a = 27.7 \pm 0.1$, $b = 8.1 \pm 0.3$ for circularly polarized measurements (blue dashed line). The error bars for the parameters estimated in the model are based on the 1σ confidence interval obtained in the fit. For each V_G value we repeat the experiment more than 10 times and fit a value for g_P to each of these measurements. The error bars on the data points are standard deviations of the extracted g_P's for these measurements. (b) Change in the particle weight as a function of V_G. The dipole size of the polariton changes from 0.09 to 3.4 nm as V_G changes from 1.4 to 0.95 V (see the Supplemental Material [23]). (c) Changes of the linewidth extracted from a reflection measurement similar to Fig. 2(a), in the linear regime, for each of the points. The error bars show the 1σ confidence interval of the linewidth extracted from a fit of the reflection spectrum to a Lorentzian. (d) Change in the ratio of g_P/γ_P for the data presented in (a) and (c).

to enhance the nonlinearity by a factor of 5. We note that the enhancement of the interactions is due to three factors: enhancement of the IX content, enhancement of the dipolar nature of direct excitons, and reduced cavity content. Furthermore, this enhancement is accompanied with a reduction in polariton linewidth, allowing for a factor of 6.5 improvement in the ratio of nonlinearity to linewidth (g_P/γ_P). In these experiments we are limited to the range $V_G \geq 0.95$ V by the light-induced changes in the charge environment in our sample.

Changes in the polariton interactions are captured by a simple model that assumes $g_P = a(|x|^4 + b|y|^4)g_0$. As shown in Fig. 4(a), measurements using linear ($a = 17.6 \pm 0.1$ and $b = 7.4 \pm 0.5$) and circularly polarized light ($a = 27.7 \pm 0.1$ and $b = 8.1 \pm 0.3$) agree with this simple model. The coefficient b characterizes the ratio of IX-IX interactions to DX-DX interactions. The difference in the estimate of $a = 17.6 \pm 0.1$ for the linearly polarized light and 14 ± 1 that was used for position-dependent measurement is due to the residual effect of the local charge environment. The value of b we determine is comparable to the ratio of the (direct) dipole-dipole interaction for IXs [19,20,29,30] to the exchange-based interaction for DXs [7,8]: $(e^2 d/\epsilon)/(6E_B a_B^2) \sim 30/6 = 5$, where ϵ is the electric permittivity in GaAs, and E_B and a_B are the binding energy and the Bohr radius of the DX. However, such an estimate does not account for the spin characteristics of excitons, the induced dipole moment of the DX exciton, or the contribution of exchange to the IX interactions [19,20,29,30]. We emphasize that our low-duty-cycle pulsed experiments, carried out using resonant excitation in a microcavity with coupled quantum well structures, yield a substantially smaller polariton interaction strength compared to recent measurements under nonresonant excitation obtained with induced dipoles in wide quantum wells embedded in waveguide structures [21,31].

Our experiments unequivocally demonstrate that the interactions between polaritons can be substantially enhanced by increasing the size of their permanent dipole moment. These strong interactions when combined with the decrease in the polariton linewidth with IX content measured in Fig. 4(b) allowed us to increase the ratio of interaction strength between dipolar polaritons to their linewidth by a factor of 6.5. A detailed analysis of our methods and results indicates that the factor of 5 increase of g_P is a lower bound on the enhancement of the nonlinearity, and an estimate based on the blueshift of the polariton resonance in a two-laser experiment yields an enhancement of g_P by a factor of 10 (see the Supplemental Material [23]). The resulting strong interactions could lead to the observation of strong quantum correlations of polaritons [32] when combined with state-of-the-art zero-dimensional (0D) cavities [16,33,34]. Moreover, their permanent dipole moment provides new perspectives for the electrical confinement of dipolar polaritons [35–38]: the resulting 0D polaritons could combine narrow linewidths of dipolar polaritons with confinement dimensions smaller than ~600 nm using appropriate gate design [39]. In addition, electrically defined lattices of 0D dipolar polaritons allow

for the tunability of on-site interaction strength to polariton-hopping ratio, while allowing for the realization of artificial gauge fields for polaritons [40]. Even though the experiments we report are based on GaAs-based heterostructures, our advances can be directly applied to van der Waals heterostructures [41,42] to realize dipolar polaritons of transition-metal dichalcogenide heterobilayers embedded in dielectric cavities.

The authors acknowledge insightful discussions with Thomas Fink and Jacqueline Bloch. This work is supported by NCCR QSIT and an ERC Advanced Investigator Grant (POLTDES).

E. T. and H.-T. L. contributed equally to this work.

[1] J. D. Pritchard, D. Maxwell, A. Gauguet, K. J. Weatherill, M. P. A. Jones, and C. S. Adams, Phys. Rev. Lett. **105**, 193603 (2010).
[2] T. Peyronel, O. Firstenberg, Q.-Y. Liang, S. Hofferberth, A. V. Gorshkov, T. Pohl, M. D. Lukin, and V. Vuletić, Nature (London) **488**, 57 (2012).
[3] Y. O. Dudin and A. Kuzmich, Science **336**, 887 (2012).
[4] D. Tiarks, S. Baur, K. Schneider, S. Dürr, and G. Rempe, Phys. Rev. Lett. **113**, 053602 (2014).
[5] H. Gorniaczyk, C. Tresp, J. Schmidt, H. Fedder, and S. Hofferberth, Phys. Rev. Lett. **113**, 053601 (2014).
[6] N. Jia, N. Schine, A. Georgakopoulos, A. Ryou, L. W. Clark, A. Sommer, and J. Simon, Nat. Phys. **14**, 550 (2018).
[7] C. Ciuti, V. Savona, C. Piermarocchi, A. Quattropani, and P. Schwendimann, Phys. Rev. B **58**, 7926 (1998).
[8] F. Tassone and Y. Yamamoto, Phys. Rev. B **59**, 10830 (1999).
[9] J. Kasprzak, M. Richard, S. Kundermann, A. Baas, P. Jeambrun, J. M. J. Keeling, F. M. Marchetti, M. H. Szymańska, R. André, J. L. Staehli, V. Savona, P. B. Littlewood, B. Deveaud, and L. S. Dang, Nature (London) **443**, 409 (2006).
[10] G. Nardin, G. Grosso, Y. Léger, B. Pitka, F. Morier-Genoud, and B. Deveaud-Plédran, Nat. Phys. **7**, 635 (2011).
[11] D. Sanvitto, S. Pigeon, A. Amo, D. Ballarini, M. De Giorgi, I. Carusotto, R. Hivet, F. Pisanello, V. G. Sala, P. S. S. Guimaraes, R. Houdré, E. Giacobino, C. Ciuti, A. Bramati, and G. Gigli, Nat. Photonics **5**, 610 (2011).
[12] A. Amo *et al.*, Science **332**, 1167 (2011).
[13] G. Grosso, G. Nardin, F. Morier-Genoud, Y. Léger, and B. Deveaud-Plédran, Phys. Rev. Lett. **107**, 245301 (2011).
[14] K. G. Lagoudakis, B. Pietka, M. Wouters, R. André, and B. Deveaud-Plédran, Phys. Rev. Lett. **105**, 120403 (2010).
[15] M. Abbarchi, A. Amo, V. G. Sala, D. D. Solnyshkov, H. Flayac, L. Ferrier, I. Sagnes, E. Galopin, A. Lemaître, G. Malpuech, and J. Bloch, Nat. Phys. **9**, 275 (2013).
[16] G. Muñoz-Matutano, A. Wood, M. Johnson, X. V. Asensio, B. Baragiola, A. Reinhard, A. Lemaitre, J. Bloch, A. Amo, B. Besga, M. Richard, and T. Volz, arXiv:1712.05551.
[17] A. Delteil, T. Fink, A. Schade, S. Höfling, C. Schneider, and A. Imamoğlu, arXiv:1805.04020.
[18] P. Cristofolini, G. Christmann, S. I. Tsintzos, G. Deligeorgis, G. Konstantinidis, Z. Hatzopoulos, P. G. Savvidis, and J. J. Baumberg, Science **336**, 704 (2012).
[19] T. Byrnes, G. V. Kolmakov, R. Y. Kezerashvili, and Y. Yamamoto, Phys. Rev. B **90**, 125314 (2014).
[20] A. V. Nalitov, D. D. Solnyshkov, N. A. Gippius, and G. Malpuech, Phys. Rev. B **90**, 235304 (2014).
[21] I. Rosenberg, D. Liran, Y. Mazuz-Harpaz, K. West, L. Pfeiffer, and R. Rapaport, Sci. Adv. **4**, eaat8880 (2018).
[22] I. Carusotto and C. Ciuti, Rev. Mod. Phys. **85**, 299 (2013).
[23] See Supplemental Material at http://link.aps.org/supplemental/10.1103/PhysRevLett.121.227402, which includes Refs. [24–27], for details on the growth and fabrication of the sample, extraction of interaction strength from reflection data, experimental details, effect of the slow charge environment, additional measurements using pump-probe experiments, and simulation of polariton dynamics including a spatial degree of freedom.
[24] J. Wilkes and E. Muljarov, Superlattices Microstruct. **108**, 32 (2017).
[25] M. Górska, H. Wrzesińska, J. Muszalski, J. Ratajczak, and B. Mroziewicz, Mater. Sci. Semicond. Process. **5**, 505 (2002).
[26] E. Wertz, A. Amo, D. D. Solnyshkov, L. Ferrier, T. C. H. Liew, D. Sanvitto, P. Senellart, I. Sagnes, A. Lemaître, A. V. Kavokin, G. Malpuech, and J. Bloch, Phys. Rev. Lett. **109**, 216404 (2012).
[27] S. R. K. Rodriguez, A. Amo, I. Sagnes, L. L. Gratiet, E. Galopin, A. Lemaître, and J. Bloch, Nat. Commun. **7**, 11887 (2016).
[28] A. Baas, J. P. Karr, H. Eleuch, and E. Giacobino, Phys. Rev. A **69**, 023809 (2004).
[29] A. V. Nalitov, M. Vladimirova, A. V. Kavokin, L. V. Butov, and N. A. Gippius, Phys. Rev. B **89**, 155309 (2014).
[30] O. Kyriienko, E. B. Magnusson, and I. A. Shelykh, Phys. Rev. B **86**, 115324 (2012).
[31] I. Rosenberg, Y. Mazuz-Harpaz, R. Rapaport, K. West, and L. Pfeiffer, Phys. Rev. B **93**, 195151 (2016).
[32] O. Kyriienko, I. A. Shelykh, and T. C. H. Liew, Phys. Rev. A **90**, 033807 (2014).
[33] T. Fink, A. Schade, S. Höfling, C. Schneider, and A. Imamoglu, Nat. Phys. **14**, 365 (2018).
[34] S. R. K. Rodriguez, W. Casteels, F. Storme, N. Carlon Zambon, I. Sagnes, L. Le Gratiet, E. Galopin, A. Lemaître, A. Amo, C. Ciuti, and J. Bloch, Phys. Rev. Lett. **118**, 247402 (2017).
[35] G. J. Schinner, E. Schubert, M. P. Stallhofer, J. P. Kotthaus, D. Schuh, A. K. Rai, D. Reuter, A. D. Wieck, and A. O. Govorov, Phys. Rev. B **83**, 165308 (2011).
[36] A. G. Winbow, J. R. Leonard, M. Remeika, Y. Y. Kuznetsova, A. A. High, A. T. Hammack, L. V. Butov, J. Wilkes, A. A. Guenther, A. L. Ivanov, M. Hanson, and A. C. Gossard, Phys. Rev. Lett. **106**, 196806 (2011).
[37] G. Chen, R. Rapaport, L. N. Pffeifer, K. West, P. M. Platzman, S. Simon, Z. Vörös, and D. Snoke, Phys. Rev. B **74**, 045309 (2006).

[38] A. Gärtner, L. Prechtel, D. Schuh, A. W. Holleitner, and J. P. Kotthaus, Phys. Rev. B **76**, 085304 (2007).
[39] G. J. Schinner, J. Repp, E. Schubert, A. K. Rai, D. Reuter, A. D. Wieck, A. O. Govorov, A. W. Holleitner, and J. P. Kotthaus, Phys. Rev. Lett. **110**, 127403 (2013).
[40] H.-T. Lim, E. Togan, M. Kroner, J. Miguel-Sanchez, and A. Imamoğlu, Nat. Commun. **8**, 14540 (2017).
[41] P. Rivera, J. R. Schaibley, A. M. Jones, J. S. Ross, S. Wu, G. Aivazian, P. Klement, K. Seyler, G. Clark, N. J. Ghimire, J. Yan, D. G. Mandrus, W. Yao, and X. Xu, Nat. Commun. **6**, 6242 (2015).
[42] M. Sidler, P. Back, O. Cotlet, A. Srivastava, T. Fink, M. Kroner, E. Demler, and A. Imamoglu, Nat. Phys. **13**, 255 (2016).